Phase transitions in $RbCaF_3$†

F. A. Modine, E. Sonder, and W. P. Unruh*
Solid State Division, Oak Ridge National Laboratory, Oak Ridge, Tennessee 37830

C. B. Finch and R. D. Westbrook
Research Materials Program, Oak Ridge National Laboratory, Oak Ridge, Tennessee 37830
(Received 31 January 1974)

Single crystals of $RbCaF_3$ have been successfully prepared by a Bridgeman method. The crystals are found to have the cubic perovskite structure at ambient temperature, but the structure is of lower symmetry at temperatures below 198 K. At lower temperatures the polarizing microscope reveals optical birefringence and well-defined domain structure. Detailed measurements of the birefringence and the paramagnetic resonance of impurity Fe^{3+} show a transformation to a tetragonal structure at 198 °K. This phase transition is at least near second order and appears similar to the antiferroelectric transitions known in $SrTiO_3$ and $KMnF_3$ (the latter has a small first-order contribution) except very near T_c where it differs from both. The measurements imply a temperature variation of the transition order parameter that is described by a critical index β which is close to 0.25 very near T_c, roughly 0.33 at somewhat lower temperature, and 0.50 or Landau-like at still lower temperatures. Preliminary measurements of the dielectric function and specific-heat anomalies have also been made. Only small anomalies are found at 198 K. However, these measurements along with the paramagnetic-resonance measurements suggest that other phase transitions occur at about 43 and 10 K.

I. INTRODUCTION

Oxides having the perovskite structure (for example, the titanates) have been of great interest because their large dielectric constants give rise to a host of properties having commercial applications and because these useful properties arise in phase changes that are of intrinsic interest.[1] It has been demonstrated that similar phase changes take place in some halide analogs of the perovskite oxides. However, only a few of the many possible compounds of the type M^+, M^{++}, X_3^-, where M represents a cation and X a halide, have been prepared and investigated, and there has yet been no demonstration that these materials become ferroelectric as do some of the oxides.

This report contains a description of a method for preparing the compound $RbCaF_3$, as well as the results of an investigation of a number of its properties. Optical birefringence, dielectric function, and heat-capacity measurements are presented along with a study of the electron paramagnetic resonance (EPR) of impurity iron in the crystals. These results are self-consistent, and show that a structural phase change from cubic to tetragonal occurs when $RbCaF_3$ is cooled below 198 K and further changes occur below 50 K. The transition at 198 K is at least near second order and appears to be analogous to the 105-K antiferroelectric transition in $SrTiO_3$.[2]

II. CRYSTAL PREPARATION

The crystals were prepared by a Bridgeman technique from high-purity powders of RbF (Research Organic/Inorganic Chemical Company) of stated > 99.9% purity and CaF_2 (Alfa Inorganics) of stated > 99.97% purity. These were accurately weighed in a dry box and mixed in stoichiometric proportions to make individual batches of approximately 20 g for each growth experiment. The mixtures were inserted in conical-bottomed platinum ampules (2-cm diameter × 6 cm × 0.5-mm wall thickness), which were then welded shut under roughing pump vacuum. The charged ampules were heated to approximately 50° above the melting point of $RbCaF_3$ (1110 °C)[3] and subsequently lowered to room temperature through a temperature gradient of 20 °C/cm at rates of 1 to 3 mm/h. In a variation of the technique, unsealed, high-density graphite containers were used under 2-atm pressure of either pure argon or helium containing 5% hydrogen by volume. In some cases, 5-wt% NH_4HF_2 was added to the melt to assist in the removal of extraneous moisture or oxygen from the starting materials during heat-up; however, this does not appear to be a necessary step for good crystal-growth results if oxygen is kept from the system and starting materials.

For the most part, polycrystalline ingots were produced by these methods. The synthesis in sealed platinum vessels produced several crystals > 1 cm^3. A rather slow-growth rate appeared to be necessary to produce reasonably large single-crystal grains. It was possible to cleave and cut the ingots to obtain single crystals of good optical quality measuring of the order of 4 × 4 × 1 mm. The crystals contained a number of impurities which came primarily from the starting materials. Predominant contaminants of one ingot are listed in Table I. We believe that purer crystals can be

TABLE I. Major impurities in $RbCaF_3$ crystals as obtained from Spark spectral analyses.

	Approximate concentration (ppm)
Al	100
Fe	10
K	1000
Mg	20
Na	100
Cs	100

grown, if the RbF and CaF_2 starting materials are first purified.

III. VISUAL OBSERVATIONS

The polarizing microscope allows the direct visual observation of phase transformations and the formation of domain structure in crystals such as $RbCaF_3$.[4] A structural phase change in an isotropic crystal introduces anisotropy and thereby birefringence which can be readily observed with polarized light. When the optic axes of twins are different, the domain structure can be optically resolved.

In order to observe the $RbCaF_3$ crystals at low temperature, the tail section of an optical, cold-finger cryostat was mounted on a small optical bench equipped with a lamp, polarizers, microscope, camera, and other accessories. The microscope could focus on the crystal through a dichroic analyzer and the cryostat window. The crystal temperature could be measured with either a GaAs diode or a germanium resistance thermometer, both mounted on the cold finger near the sample.

When viewed between crossed polarizers, thin crystals (e.g., typical dimensions: $4\times4\times1$ mm) of $RbCaF_3$ were found to be optically isotropic at room temperature. Good extinction was obtained for the crossed polarizers at any angle with respect to the crystal. The extinction was much better than that for similar crystals of $SrTiO_3$, a material previously found somewhat anisotropic at room temperature.[5]

The $RbCaF_3$ crystals remained optically isotropic as the temperature was reduced until an onset of birefringence occurred at approximately 198 K. The onset was gradual, but the crystals became bright over a very small range in temperature. As the crystal became bright, a pattern of striations oriented in a [110] direction developed. It was still possible to obtain good extinction with the crossed polarizers when they were oriented in crystallographic [100] directions. This indicated that the optic axis of the newly formed structure was in the surface of the crystal and was oriented in one of the [100] directions.

A photograph of a typical striation pattern is shown as Fig. 1. The striations can be interpreted as 90° domain boundaries of the crystal tetragonal phase. If the crystal is viewed with the polarizers near their [100] extinction positions, the striations appear to move slightly when the polarizer is rocked. A quarter-wave plate interposed before the crystal similarly causes a motion in the striations as the wave plate is moved. This probably is a result of strain at the domain boundaries.[4] In regions of the crystal where perpendicular sets of striations meet, a closure of the open ends, which gives a spear-point pattern, is often observed. Most domains appear to extend completely through the crystal, but overlapping patterns have been observed. The widths of single domains appear greatly variable, but are typically of the order to 50 μ. A continuous change in the width of the domains with temperature, such as occurs in $KMnF_3$,[6] was not observed. However, gross rearrangement of the domains was infrequently noticed. Near the transition, it was possible to follow with a monochromator the expected blue to red variation in the color of the light transmitted by individual domains as the temperature was reduced.

IV. OPTICAL-BIREFRINGENCE MEASUREMENTS

Quantitative measurements of optical birefringence are usually made by utilizing a phase compensator or polarimeter. However, because ex-

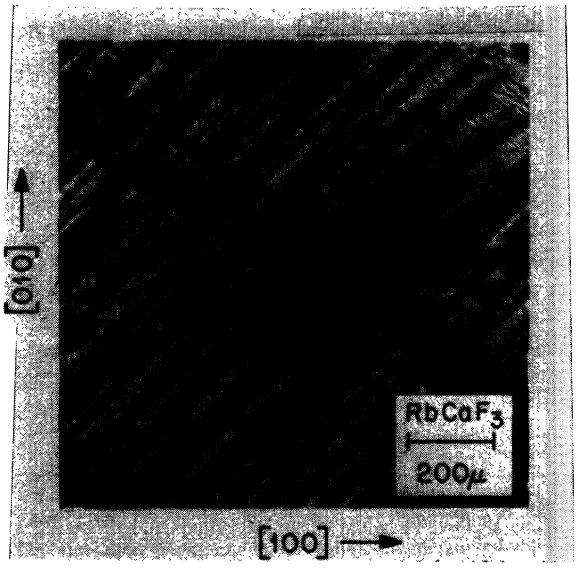

FIG. 1. Typical domain pattern of $RbCaF_3$ below 198 K.

isting laboratory equipment[7] could be conveniently adapted, a high-frequency light modulation method was used. The application of this technique does not require single domain crystals and can give very high sensitivity. Less than 10^{-3} deg of relative phase retardation can be detected.

The optical arrangement and a detailed discussion of the method is given elsewhere.[8] Essentially, the polarization of a beam of monochromatic light is modulated by a photoelastic modulator which converts linearly polarized light into light oscillating between left- and right-ellipticity at 50 kHz. Birefringence in the sample crystal biases this oscillatory polarization, creating an intensity variation at the modulation frequency in the beam which emerges from an analyzing polarizer. This variation in light intensity is detected by a photomultiplier tube and measured with a lock-in amplifier. The output signal S which is proportional to the 50-kHz variation of the photomultiplier current is given by

$$S(\lambda, \Delta n) = K \sin\gamma \quad , \tag{1}$$

where γ is the relative phase retardation of the sample and K is a combination of experimental parameters that are adjusted by the equipment control circuitry to keep K constant.[7] The birefringence, which may be defined as the difference in the crystal refractive index (Δn) for light polarized perpendicular and parallel to the optic axis, is related to γ,

$$\gamma = \frac{2\pi \Delta n t}{\lambda} = \frac{E \Delta n t}{\hbar c} \quad , \tag{2}$$

where t is the crystal thickness and E is photon energy.

Equation (2) gives an accurate description of the measurement only if the crystal exhibits a uniform birefringence. In a multidomain crystal, such as considered here, the resultant signal is a superposition derived from the various domains, and the term $\sin\gamma$ of Eq. (2) must consequently be averaged over the crystal. Since the domain structure is random and twins have birefringence of opposite sign, the statistical expectation of a measurement is zero. However, it is not expected statistically, nor found experimentally, that an individual measurement gives zero signal. The opposing contributions do not usually exactly cancel. The signal intensity is, of course, diminished, but for the moment it is adequate to assume that the significant effect of multiple domains is to reduce the signal by a random factor, which may be incorporated into the constant K.

Since the birefringence is a function of temperature T the detected signal is a function of both λ and T. Experimental measurements were conveniently made by changing one of these variables, while keeping the other constant. Figure 2 shows some results of measurement; the signal intensity is given as a percentage of the signal obtained from a mica quarter-wave plate. The figure shows a particularly large signal, however, all measurements gave a maximum signal intensity of at least 1%. The signal amplitude for different samples appeared to be random, but individual measurements were usually reproducible for any given crystal, if it was not warmed to more than a few degrees above the transition temperature. Warming the crystal to higher temperatures before recooling gave a different signal intensity. In one of the four crystals measured, gross domain rearrangement occurred as the temperature changed. This resulted in nonreproducible step discontinuities in the measured signals.

The oscillatory signals are not strictly of constant amplitude and hence are described only approximately by Eqs. (1) and (2). Ignoring for the moment the deviation from a pure harmonic behavior, it is possible to interpret the signal zeros as corresponding to a retardation of $m\pi$ rad, where m is an integer. The temperature and energy dependence of the retardation, such as shown in Fig.

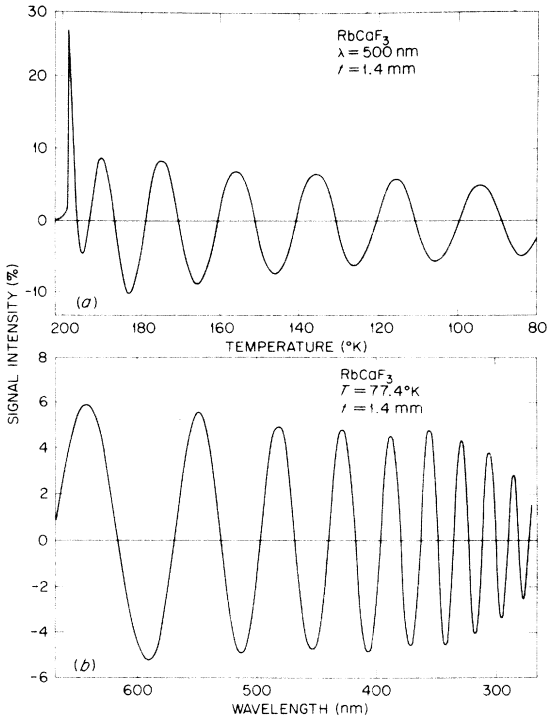

FIG. 2. Recorded signal vs sample temperature (a) and light wavelength (b) for a 1.4-mm-thick $RbCaF_3$ sample.

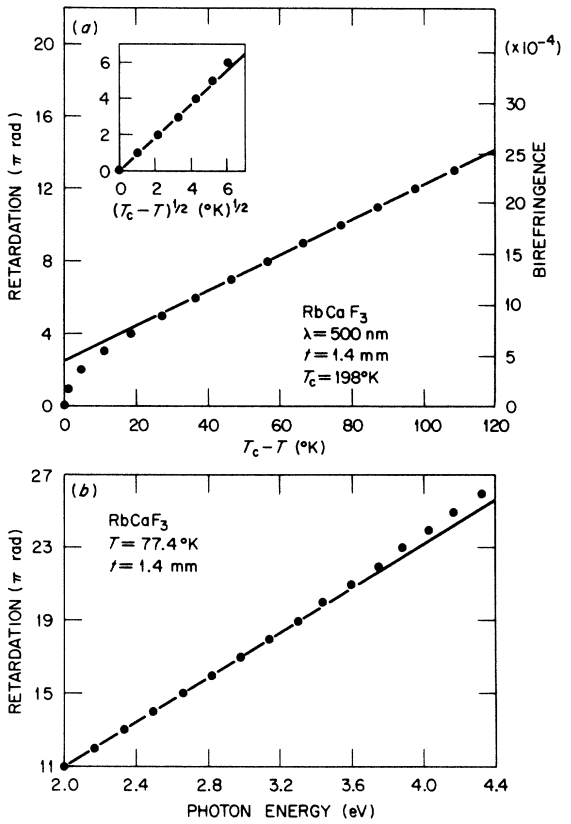

FIG. 3. Relative retardation of polarized components of incident light vs sample temperature (a) and spectral energy (b). These results were derived from the data shown in Fig. 2.

3, can thus be plotted. Measurement of the sample thickness yields values of the birefringence as shown by the right-hand scale of Fig. 3(a). The birefringence varies almost linearly with temperatures over most of the range of measurements. However, as shown by the inset of Fig. 3(a), it appears to have an approximate square-root dependence on $T_c - T$ in the critical region near the transition temperature (T_c). At lower temperatures than the measurements shown, $\Delta n(T)$ saturates as expected from thermodynamics considerations. It was found to be well saturated at liquid-helium temperature. The variation of the retardation with photon energy is nearly linear at all temperatures and corresponds to Eq. (2). The small deviation from linearity is probably due to a small wavelength dependence of the birefringence (Δn). The birefringence, like the index of refraction, can be expected to increase as the band edge is approached.

Let us now consider more rigorously the effects of the domain structure. For a crystal having domains, the retardation [Eq. (2)] is a function of position,

$$\gamma(x,y) = (2\pi/\lambda) \int \Delta n(x,y,z)\,dz \quad . \tag{3}$$

An effective optical-path difference can be defined for each point (x,y) on the crystal surface, this being the net excess of thickness of one type of domain over the other or

$$t(x,y) = \int \frac{\Delta n}{|\Delta n|}\,dz \quad . \tag{4}$$

The observed signal is then simply the sum of signals due to the various path differences for the illuminated part of the crystal surface or

$$\begin{aligned} S &= \frac{K}{A}\int \sin\gamma(x,y)\,dx\,dy \\ &= \frac{K}{A}\int \sin\left(\frac{E}{\hbar c}\,|\Delta n|\,t(x,y)\right)dx\,dy \\ &= K\int N(t)\sin\left(\frac{E}{\hbar c}\,|\Delta n|\,t\right)dt \quad , \end{aligned} \tag{5}$$

where $N(t)$ is a distribution of optical paths over the sample of area A. Equation (5) shows that in general, the measured signals will contain a distribution of frequencies. This explains the shape of the signals. When $|\Delta n|$ is very small—which it is near the transition temperature, or when E is very small—there is a phase coherence of the various components; as a result large signals are observed. However, at lower temperature or shorter wavelengths, coherence becomes less and the signals decrease. Since the signals do not vanish, the distribution obviously contains well-defined peaks. This is what one would expect from the visual observations which indicated that most of the domains penetrated through the thickness of the plates, i.e., that $N(t)$ peaked at $t = \pm T$, the crystal thickness. An experiment to determine whether the retardation scaled with crystal thickness confirmed that the predominant domain depth was T and implied that the use of the actual crystal thickness in determining the (right) ordinate scale for $\Delta n(T)$ of Fig. 3 gives near-correct values.

It may be of interest to note that Fig. 2 shows a small birefringence tail above the transition temperature. This tail may be due to inhomogeneities which slightly perturb the transition temperature in some regions of the crystals or it may be due to some orienting mechanism which determines the domain structure by favoring certain fluctuations. Such an orienting mechanism would explain the reproducibility of measurements in crystals warmed to only a few degress above the transition temperature and then recooled. The later explanation has recently been proposed for the birefringence tail found in $SrTiO_3$,[9] where it gives an explanation of

a small cusp found at the transition temperature. No attempt was made to find a similar cusp in the $RbCaF_3$ birefringence. Neither temperature stability nor the multidomain samples would have been conducive to such an attempt.

Considering now the wavelength and temperature dependence of the signal S let us assume that the wavelength dependence enters only through the explicit factor E in Eq. (5) and the temperature dependence enters only through $|\Delta n|$ and is of the form:

$$|\Delta n(T)| = \Delta n_0 (T_c - T)^{2\beta} \quad . \tag{6}$$

We can find a relationship between E, $|\Delta n(T)|$, and S that is independent of the domain structure. Applying the identity,

$$\left(\frac{\delta E}{\delta T}\right)_S = -\left(\frac{\delta S}{\delta T}\right)_E \Big/ \left(\frac{\delta S}{\delta E}\right)_T \quad , \tag{7}$$

to Eq. (5), in which $|\Delta n(T)|$ has been given the functional dependence specified by Eq. (6), yields

$$\left(\frac{\delta E}{\delta T}\right)_S = 2\beta E/(T_c - T) \quad , \tag{8}$$

which can be integrated, giving

$$\ln E = -2\beta \ln(T_c - T) + \ln F(S) \quad , \tag{9}$$

where $F(S)$ is a constant function. The zeros are the most easily followed constant amplitude signals and Fig. 4 shows a logarithmic plot of these as a function of E and T. From the slope of the lines a value of $2\beta = 0.61 \pm 0.06$ is computed for the range $5 < T_c - T < 35$ K.

V. EPR MEASUREMENTS

The study of substitutional transition-series ions in perovskite crystals has provided a great deal of information on lattice phase transitions in these materials.[10-13] In the case of $SrTiO_3$, EPR-line splitting constituted the initial evidence[13] for the structural phase transition at 105 K and provided the initial geometrical picture of the cubic-tetragonal transition[11] and the identification of the order parameter as a rotation of the oxygen octahedra.[12]

We have studied the EPR spectrum of Fe^{3+} impurity ions in $RbCaF_3$ throughout the temperature range 1.1–350 K, with particular emphasis on the range from 77 to 300 K. Measurements were made on two different x-band EPR spectrometers. In the temperature range above 80 K, a homodyne video spectrometer equipped with a Varian gas-flow temperature-control system was used, while the region below 80 K was investigated by means of a superheterodyne spectrometer operating with the cavity in a double Dewar system. Temperatures below 80 K were measured by means of a calibrated platinum resistor on the cavity wall. In the gas-flow system a copper-constantan thermocouple was glued directly onto the crystal (the cavity mode is undisturbed, since the leads enter along the axis of the gas flow, which is in the region of minimum E field). The calibrations of both thermometers were checked against a series of Freons, dry ice, and liquid nitrogen and helium, and were consistent to ± 0.5 K throughout the temperature ranges studied in each case.

Crystals obtained from different sample preparations varied significantly in incidental iron-impurity content. In some crystals the major impurity was, in fact, manganese, which exhibited a far smaller axial splitting than that observed for the iron. The crystals used in this work were typically $1 \times 2 \times 4$ mm in size and came predominantly from a boule which contained a significant amount of iron. The Fe^{3+} spectrum was quite weak in as-grown samples, but could be increased dramatically and saturated by a short irradiation with ^{60}Co γ rays. Crystals stored at room temperature exhibit a fading of the Fe^{3+} spectrum with a half-life of a few days. On the other hand, isochronal anneals carried out in a total time of $\sim \frac{1}{2}$ day show an anneal temperature of $\sim 650\ ^\circ C$, so that thermal excitation of carriers is not responsible for the annealing of the Fe^{3+} spectrum in a crystal stored at 300 K for several days.

A. Axial splitting of Fe^{3+}

The EPR spectrum of Fe^{3+} in this material is conveniently described in the irreducible tensor notation,[14] with an added superhyperfine term for describing the strong interactions with the nearest-neighbor fluorine nuclei ($I = 1/2$). In the cubic phase, the appropriate fine-structure spin Hamiltonian is

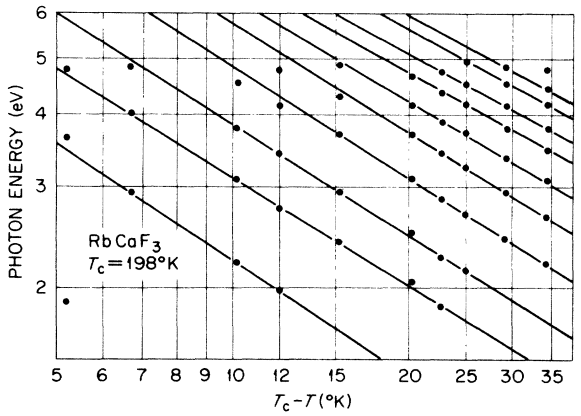

FIG. 4. Logarithmic plot of spectral energy vs sample temperature for zero signal intensity.

TABLE II. Fine-structure splittings relative to the central $(1/2 \rightarrow -1/2)$ line for Fe^{3+} in cubic and tetragonal symmetry.

Transition	Cubic	Tetragonal	
		$\theta = 0°$	$\theta = 0°$
$(\pm 5/2 \longleftrightarrow \pm 3/2)$	$\mp 4\, b_4^0$	$\mp 4\, b_4^0 \pm 4\, b_2^0$	$\mp 4\, b_4^0 \pm 2(b_2^0 - \frac{1}{4}\,\Delta b_4^4)$
$(\pm 3/2 \longleftrightarrow \pm 1/2)$	$\pm 5\, b_4^0$	$\pm 5\, b_4^0 \mp 2\, b_2^0$	$\pm 5\, b_4^0 \pm (b_2^0 + \frac{5}{8}\,\Delta b_4^4)$

$$H = \mu_B g_Z \vec{H} \cdot \vec{S} + \frac{b_4^0}{60}\,(O_4^0 + 5O_4^4), \tag{10}$$

where $S = 5/2$ and the tensors O_n^m are linear combinations of spin operators. Evaluation of the first two terms in this Hamiltonian gives the transition energies, to first order:

$$\begin{aligned} \Delta E(\pm 5/2 \rightarrow \pm 3/2) &= G \pm 4\, b_4^0 \quad , \\ \Delta E(\pm 3/2 \rightarrow \pm 1/2) &= G \mp 5\, b_4^0 \quad , \\ \Delta E(+1/2 \rightarrow -1/2) &= G \quad , \end{aligned} \tag{11}$$

where $G = \mu_B g_z H_z$. Because of the large superhyperfine splittings in the spectrum, these fine-structure transitions energies can be measured with much less precision in this case than has been possible in comparable situations in the oxide perovskites. Second-order effects on G which develop with the observed splittings are quite small compared to these splittings. Therefore, it is sufficient to deal only with such first-order results, and we can specify splittings in the fine-structure lines relative to G, the nominal $M_S = 1/2 \rightarrow -1/2$ transition energy.

Examination of the EPR spectrum in the cubic phase allows one to determine unambiguously the substitutional site for the Fe^{3+} ion by means of the large superhyperfine interactions with the neighboring ^{19}F nuclei. This superhyperfine structure is described by an added term $\sum \vec{I}_i \cdot \vec{A}_i \cdot \vec{S}$, with the sum over the nearest-neighbor ^{19}F nuclei which provides the dominant interactions observed. The superhyperfine linewidths for the several fine-structure components of the spectrum are quite different at temperatures below ~250 K and in particular, the $M_S = 1/2 \rightarrow -1/2$ set of superhyperfine lines sharpens rapidly with reduced temperature. For this set of lines, one observes a completely resolved splitting, for H applied along [100], corresponding to groups of four and two equivalent nuclei, with the interaction strengths nearly the dipolar values for the divalent lattice site (Ca) surrounded by a regular octahedron of six fluorines. We conclude that the Fe^{3+} ion resides substitutionally in the Ca^{2+} site (a result consistent with the comparable ionic radii of the two ions), and that the observed splittings below 198 K are a result of the distortion of this octahedron accompanying the lattice phase transition. These distortions are visible, of course, as small splittings and second-order shifts in the sharp central $M_S = 1/2 \rightarrow -1/2$ set of superhyperfine lines, but they can best be followed by looking at the fine-structure transitions themselves.

The EPR spectrum below 198 K exhibits large and temperature-dependent tetragonal splittings of Fe^{3+} fine-structure lines. A detailed examination of the various splittings shows these components exhibit domain structure, i.e., a superposition of three tetragonal single-crystal spectra, corresponding to the development of preferred axes along the three previously cubic axes. The intensity ratios encountered range from nominal equality for domains with c (unique) axes in the previously cubic axes, to ratios of more than 10:1. The high ratios appear normally in samples cleaved in the shape of thin plates; the low intensity corresponds to domains whose c axis is perpendicular to the surfaces of these plates. A particular domain ratio measured at $T < 198$ K will generally be preserved if the crystal is cycled only a few degrees above 198 K and then recooled, while crystals cycled up to ~300 K generally exhibited different domain structure upon recooling to $T < 198$ K.

The fine-structure lines in the EPR for a given domain in the tetragonal phase can be described conveniently by irreducible tensor expressions written explicitly for the two principal directions. For $\theta = 0°$,

$$H = G S_Z + \tfrac{1}{3} b_2^0 O_2^0 + \tfrac{1}{60}\,(b_4^0 O_4^0 + b_4^4 O_4^4) \quad , \tag{12}$$

and for $\theta = 90°$,

$$\begin{aligned} H = {} & G S_Z - \tfrac{1}{6}\,(b_2^0 O_2^0 + 3 b_2^0 O_2^0) + \tfrac{1}{480}\,(3 b_4^0 + b_4^4)\, O_4^0 \\ & + \tfrac{1}{120}\,(5 b_4^0 - b_4^4)\, O_4^2 + \tfrac{1}{480}\,(35 b_4^0 + b_4^4)\, O_4^4 \, . \end{aligned} \tag{13}$$

The requirement that these tetragonal expressions reduce to the cubic case in the limit as the axes become equivalent leads to the limiting relations $b_4^4 \rightarrow 5 b_4^0$, $b_2^0 \rightarrow 0$. As will be demonstrated, the EPR splittings appear gradually (at least nearly a 2nd-order transition), so one needs a way of relating the cubic and tetragonal splittings. If we let $b_4^4(\text{cubic}) \equiv b_4^4(O) = 5 b_4^0$, and then in the tetragonal phase define $b_4^4 = b_4^4(O) + \Delta b_4^4$, the disappearance of the tetragonal distortion is described by $b_2^0 \rightarrow 0$, $\Delta b_4^4 \rightarrow 0$.

For the three cases above, the splittings relative to the central $(1/2 \rightarrow -1/2)$ line are given in Table II.

Each of these fine-structure lines (as viewed along pseudocubic axes) has the superimposed 15-line superhyperfine pattern of the $6mn$ ^{19}F nuclei, which has a central unshifted component. Measurements of the positions of these central components

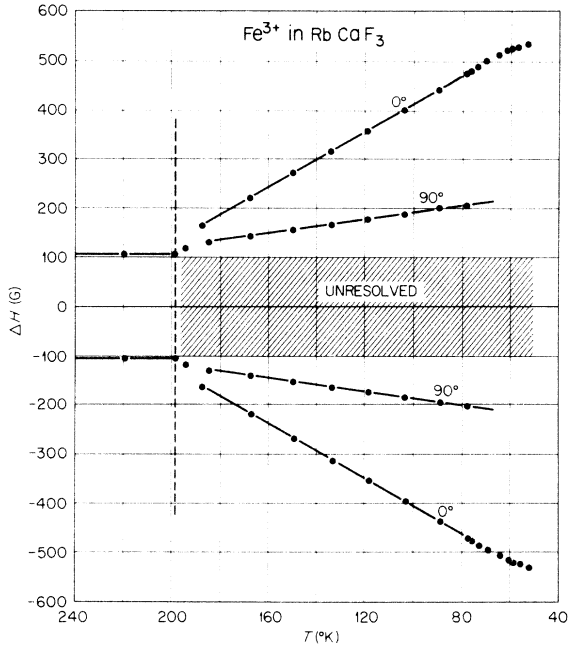

FIG. 5. Temperature dependence of the position of the central component of Fe^{3+} fine-structure lines in $RbCaF_3$.

versus temperature are shown in Fig. 5. The spectrum observed with H applied along [100] consists of a widely split cubic spectrum for $T > T_c$, which then progressively develops both $\theta = 0°$ and $90°$ splittings as T is lowered. The plotted points are the field positions, relative to G, of the central superhyperfine components of each fine-structure line. Only the outside splittings of the $\theta = 90°$, $M_S = \pm 3/2 \leftrightarrow \pm 1/2$ transitions and the $\theta = 0°$, $M_S = \pm 5/2 \leftrightarrow \pm 3/2$ are visible. The other splittings are toward the central $M_S = 1/2 \leftrightarrow -1/2$ transitions and become completely lost in the unresolved tangle of superhyperfine lines at the center of the spectrum (becoming marginally visible again for $T < 90$ K).

The linear splitting evident for much of the temperature range of Fig. 5 can be accounted for very successfully on the assumption that the parameter b_4^0 does not change from the value it has in the cubic crystal ($b_4^0/g\mu_B = 22.1$ G) when the sample becomes tetragonal, and that the tetragonal parameters, Δb_4^4 and b_2^0 vary linearly with $(T_c - T)$. The resulting two-parameter fit shown as a solid line in Fig. 5 is for $\Delta b_4^4/g\mu_B = -0.391 + 0.021\ (T - T_c)$ and $b_2^0/g\mu_B = 11.60 + 0.619(T_c - T)$. The signs are chosen by observing the spectrum at 1.2 K, where b_2^0 is determined to be positive on the basis of the thermal populations of the fine-structure components. This fit shows that $b_2^0(T)$ is by far the dominant term in the linear temperature-dependence range. (In fact, the small $\Delta b_4^4(T)$ deduced from the fit may not be real, and an acceptable fit could probably be achieved with $\Delta b_4^4 = 0$.) The temperature dependence of $b_2^0(T)$ is shown in Fig. 6.

B. Temperature dependence near cubic-tetragonal transition temperature

As seen in Figs. 5 and 6 the validity of the linear fit does not extend to the transition temperature. It is of some interest to detail the behavior of the splittings in the region of the transition temperature, and to determine whether any discontinuity in the splittings is visible at the transition. Inspection of the expected splittings given in Table II shows that the $\theta = 90°$ $(+3/2 \leftrightarrow +1/2)$ transition, which is the high-field line, shifts upward in field as a nonzero b_2^0 develops. Because the superhyperfine structure on this line is rather broad, direct measurements of small shifts versus T are difficult to make. We have instead done a slow temperature scan at fixed magnetic field, and used the superhyperfine structure itself as an "interference pattern" to scan the line shift due to the developing b_2^0. This method is described briefly as follows.

A high-resolution EPR trace of the last few superhyperfine lines at the high-field edge of the resonance is made at $T \gtrsim T_c$. Then the magnetic field is adjusted to the zero-derivative crossing of the highest-field superhyperfine line and a slow temperature scan down through the transition tem-

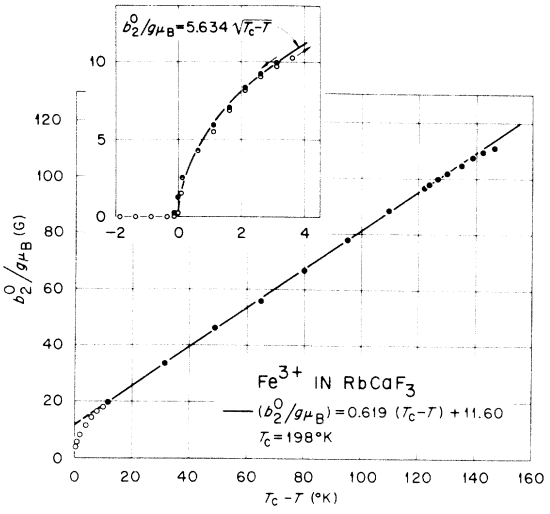

FIG. 6. Temperature dependence of the parameter b_2^0 for the fine-structure splitting of Fe^{3+} impurity in $RbCaF_3$. The region near the transition temperature is expanded in the inset. The open and full circles in the main figure indicate data obtained in several experiments; in the inset they indicate decreasing and increasing temperature, respectively. The lines are drawn according to the indicated functions.

perature is initiated. In our case, this was done by slowly driving the temperature-control dial on the standard Varian gas-control system so as to produce a temperature change of ~1 K/min. An X-Y recorder plotted the resulting EPR derivative signal versus temperature, which consisted of the superhyperfine pattern scanned upward through the constant magnetic field value by the progressive increase of b_2^0. Unfolding this derivative signal by means of the previously recorded cubic spectrum gave the progressive values of b_2^0 versus temperature.

The result of one such scan is shown in the inset of Fig. 6 for both decreasing and increasing temperature through the transition. For the results shown in the inset of Fig. 6, it has been assumed that Δb_4^4 is unchanged over the 4°-temperature range. The thermocouple used to measure T was glued onto the sample and calibrated as previously discussed. The temperature fluctuations of the sample, as seen by the thermocouple, were ~0.2 K rms, and an over-all stability of ~0.3 K over 50 min was possible. Since the onset of the transition can be seen with great sensitivity under nearly static conditions, these observations provide our best measurement of the transition temperature, which is $T_c = 198.0 \pm 0.5$ K. They also show that there is no appreciable discontinuity or hysteresis in the transition and that $b_2^0(T)$ follows a nominal $(T_c - T)^{1/2}$ dependence for about 10 K, until the apparently linear splitting takes over below about 190 K.

C. Low-temperature behavior

Measurements between liquid-nitrogen and liquid-helium temperatures indicate that the crystal-field parameters do not continue in the linear behavior depicted in Fig. 5 but undergo rather abrupt changes at 43 K and near 10 K. These changes are accompanied by much hysteresis. They appear to be reflections of additional phase changes, as is substantiated by corresponding changes in the dielectric and specific-heat behavior as discussed below. However, they are not apparent in the birefringence.

The EPR spectrum of Fe^{3+}, when viewed during the cooling part of a cycle from 77 to ~6 K, appears to remain tetragonal with the domain structure it had at 77 K. This symmetry and domain structure are inferred largely from the $M_S = 1/2 \leftrightarrow -1/2$ set of superhyperfine lines, on which one sees the corresponding second-order splittings very well-resolved because of the narrow linewidths. The other fine-structure components appear to lose intensity drastically, especially in the 50-K↔20-K range, although this effect was difficult to observe because of problems associated with producing a slow and steady cooling in our Dewar system. However, at ~6 K, the EPR is definitely tetragonal, with a somewhat larger splitting than it had at 77 K, and the fine-structure lines are visible.

As the sample is warmed up slowly from 6 K, several remarkable changes take place in the EPR spectrum. Between 10 and 20 K the outer fine-structure lines completely disappear, leaving just the $M_S = 1/2 \leftrightarrow -1/2$ central transition. Coincidentally, that part of the central-transition spectrum corresponding to resonance in domains oriented with their tetragonal axes parallel to the applied magnetic field also disappears, leaving behind a spectrum that appears cubic in all respects. This residual spectrum is independent of temperature between ≃ 20 K and 43 K. At $T = 43.0 \pm 0.2$ K, as the sample is warmed, the previously missing part of the central $M_S = 1/2 \leftrightarrow -1/2$ resonance spectrum abruptly reappears over a narrow temperature range (~0.2 K), as do the remaining fine-structure lines for both a and c domains. This unusual behavior is suggestive of at least one more low temperature lattice transformation, an inference which is reinforced by the observation that the domain structure (i.e., the ratio of c to a domain volume) is different after the sample has been cycled from 77 to 6 K and back up through 43 K than it was initially at 77 K. Except for this different domain structure, the EPR splitting behaves reversibly as the sample is warmed from 43 to 198 K. The detailed understanding of this unusual behavior will require better temperature control than was available at present.

It is interesting to note that similar loss of resonance intensity was seen in the EPR of Gd^{3+} in $BaTiO_3$, and the suggestion made in that case[10] that the optical-mode condensation at zero frequency was responsible for a lifetime broadening of the EPR resonance beyond detectability as the phonon frequency decreased through the microwave region of the spectrum.

VI. MEASUREMENTS OF DIELECTRIC PROPERTIES

Cooperative lattice transitions are expected to give rise to discontinuities or other changes in dielectric properties as, for example, the change in slope of dielectric constant with temperature that occurs for the case of $SrTiO_3$.[15]

Audiofrequency measurements were made at 10 kHz with a General Radio model 2990-9248 automatic impedance bridge which permitted simultaneous recording of capacitance and loss. The impedance bridge provided digital readout and automatic ranging of both capacitance and loss, as well as the capability of biasing the capacitor with voltages of up to 40 V during measurement. Normally a measuring amplitude of ~5 V rms was applied to the capacitor. The bridge readings

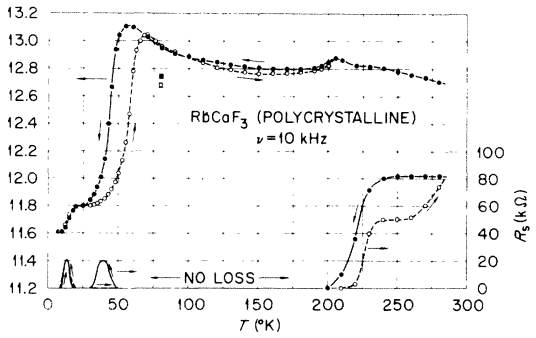

FIG. 7. Audiofrequency dielectric constant and loss of polycrystalline $RbCaF_3$ vs temperature. The solid lines and points indicate measurements made during cooling; the dashed lines and open circles indicate measurements made while the sample was warming.

were applied to the Y_1, Y_2 axes of a dual X-Y recorder, and the resistance of the calibrated Pt thermometer was used to drive the X axis. A relatively large slice of $RbCaF_3$ (area: 0.51 ± 0.06 cm^2, thickness: 0.061 ± 0.005 cm) was cut from a polycrystalline boule. Electrodes were applied with a silver-elastomer material, Eccocoat Flexible Elastomer (Emerson and Cummings Inc.) type CC4, and the platinum resistance thermometer was bonded to the outside of one of these electrodes with Dow-Corning type 340 heat-sink compound. This assembly was mounted inside a cylindrical thermal shield which had a heater wound on its outside surface and was suspended in a Dewar system. Connection to the bridge was made with 50-ohm thin-walled stainless-steel coaxial lines from the thermal enclosure to the Dewar header; all other leads were in contact with a suitable heat sink before entering the enclosure. The temperature of this capacitor could be slowly cycled between 300 and 77 K and between 77 and 6 K by the appropriate combinations of heater power, exchange gas, and liquid nitrogen or helium transferred into the Dewar system.

Measurements at 9.5 GHz were made by the conventional resonant-cavity perturbation methods,[16] but no attempt was made to cut samples into the ideal ellipsoidal shapes required for an absolute determination of dielectric constant and loss. Several small samples (all single crystals) were investigated by gluing each to the broad wall of the rectangular TE 102 mode cavity at the $\frac{1}{4}\lambda$ position of maximum E_{rf}. Cavity frequency shift (measured by means of an electronic counter) and relative loss (as determined from the cavity coupling) were measured as a function of temperature, and then compared to the frequency shift and loss of the empty cavity throughout the same temperature range. This procedure yielded the relative dielectric constant and loss throughout the temperature range from 300 to 80 K. Some differences were observed between samples oriented differently with respect to the cavity E field, but these were slight and could not be positively correlated with the actual domain structure present in the tetragonal phase.

Results of the audiofrequency measurements are shown in Fig. 7. Transitions in the vicinity of 200 and 40 K are clearly visible, as is the small change and accompanying loss peak at 10 K. These small changes in ϵ can be easily observed, since there is no large paraelectric behavior in ϵ. The low value, $\epsilon = \sim 12$, is accompanied by essentially no temperature dependence in ϵ except for that associated with the lattice anomalies; this is quite different from the case of the oxide perovskites,[15,17] for example. The losses accompanying the low-temperature changes in ϵ are normal in appearance, but the weak peak in ϵ at ~198 K appears to be associated with a loss in the high-temperature (cubic) phase which abruptly decreases to zero as the domain structure appears for the tetragonal phase. The mechanism responsible for this ac loss has not been found. It appears to depend upon the rms field applied to the sample during the measurement. At temperatures just above 198 K the loss decreases to nearly zero if the ac field is decreased in amplitude during the measurement, and it increases if the ac field is increased. There appears to be an electric field "annealing" effect as well, in the sense that momentarily increasing the ac measuring field at fixed temperature and then reducing it to its initial amplitude results in substantially less than the initial loss (sometimes reducing an initial loss to zero even for $T > T_c$).

The 43-K transition previously mentioned in the EPR measurements exhibits the dominant change in ϵ. There is an additional decrease of ϵ when the temperature goes below 10 K.

Attempts to see a dependence of ϵ on polarizing field or measuring field amplitude below 198 K were unsuccessful. Voltages up to ± 40 V (656 V/cm) produced no detectible change in ϵ. We also cooled the capacitor through the several transitions with its plates shorted and detected no change in ϵ determined by the first measuring cycle of the bridge.

The microwave dielectric constant and loss results are shown in Fig. 8. ϵ exhibits a reversal in slope at 198 K, and the size of this effect depends upon the relative orientation of the crystal and the microwave E field. However, no anomaly in the relative loss R_s is visible for this particular crystal, and indeed none of the crystals investigated showed any anomalous microwave loss at or above 198 K. Below 90 K the loss drops rapidly to zero and seems to remain essentially zero down to 4.2

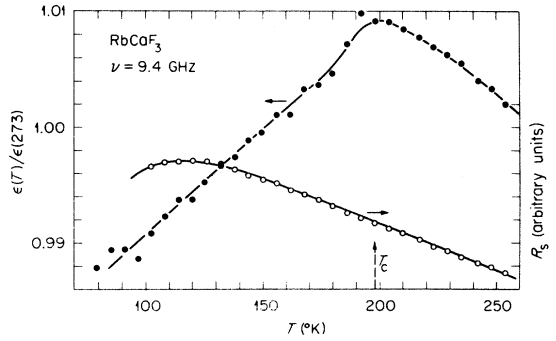

FIG. 8. Microwave dielectric constant (full circles) and loss (open circles) of $RbCaF_3$ vs temperature.

K. In particular, no anomalous cavity shifts or coupling changes were observed during high-sensitivity EPR runs as the temperature cycled through any of the transition regions indicated in Fig. 7.

VII. HEAT-CAPACITY MEASUREMENTS

Heat-capacity anomalies are well-known indicators of phase changes. Since local effects which might produce changes in the EPR would not produce any pronounced changes in the specific-heat, qualitative heat-capacity measurements, particularly in the temperature range of the unusual behavior of the Fe^{3+} resonance were deemed useful to confirm that bulk phase transitions were taking place. The measurements reported here were of a preliminary nature, done on a polycrystalline boule of $RbCaF_3$, by means of a rate of temperature drift method.

The sample was mounted on a small polyfoam support inside a thermal enclosure. This enclosure was located in the liquid-He compartment of a double Dewar system. A gold-iron versus chromel thermocouple, glued in a hole drilled into the $RbCaF_3$ boule, was used to measure the temperature difference between the sample and the thermal enclosure. The temperature of the thermal enclosure itself was measured by a calibrated platinum resistor. Specific-heat anomalies were then detected by recording the temperature differential during a slow drift in temperature of the entire apparatus.

At low temperatures the temperature drift was established by pumping away all the liquid helium after a transfer of a few cm^3 for cooling, and then allowing the thermal enclosure and the sample within it to rise toward liquid-nitrogen temperature by radiation heating from the outer Dewar of the cryostat system. For the high-temperature transition establishing a stable slow drift was more difficult and required the radiative cooling due to the liquid nitrogen in the outer Dewar to be balanced by resistance heating of the thermal enclosure around the sample.

The results of this procedure are shown in Fig. 9, where the differential temperature is plotted against the actual sample temperature. The traces, shown separately for two temperature ranges, required ~1 h each to complete. Both the 198- and 43-K transitions are evident even with this crude procedure, and show the transitions to be cooperative lattice effects involving a substantial heat-capacity change. As with the dielectric data, the 43-K transition is more prominent than that at 198 K. The nearly vertical slope of ΔT vs T at 43 K suggests a first-order transition, and is consistent with the abrupt changes seen in the EPR spectrum at this same temperature.

VIII. SUMMARY AND DISCUSSION

A. Transition at 198 K

The EPR results clearly indicate that the environment of a substitutional Fe^{+++} changes from cubic to tetragonal, and the birefringence and visual observations show that this transition is a bulk-phase transition that creates domains with $\{110\}$ (pseudocubic) walls and $\langle 100\rangle$ (pseudocubic) tetragonal axes. The temperature dependence of the splitting of the EPR lines and of the birefringence is very similar to that observed in other perovskite compounds, for example, $SrTiO_3$[18] or $KMnF_3$.[6,19]

Our birefringence and EPR measurements can be compared to previous results in oxide perovskites and in $KMnF_3$, if one makes the assumption that the 198-K phase transition arises from a similar structural transformation. In those cases the transition is the result of a condensation of one of the triply degenerate Γ_{15}' (Ref. 20) phonon modes at the Brillouin-zone R point.[21–24] The corresponding order parameter is a rotation angle ψ of the anion octahedral complex[12,18]; in $RbCaF_3$ this would be rotation of the CaF_6 octahedra around $\langle 100\rangle$ pseudocubic axes. Although we have not been able to measure directly this small angle ψ in the EPR spectra, the twinning and axial splitting

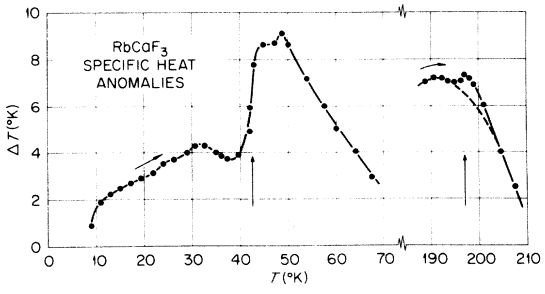

FIG. 9. Specific-heat anomalies in $RbCaF_3$.

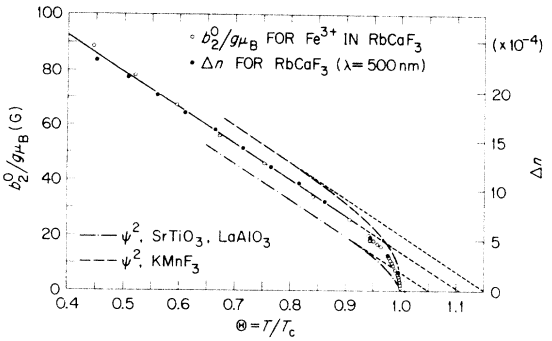

FIG. 10. Comparison of the temperature dependence of b_2^0 and Δn of $RbCaF_3$ with that of the square of the order parameter of other perovskites. The points are experimental data for $RbCaF_3$. The dashed lines correspond to values in the literature (Refs. 12 and 19) normalized so that the slope of the dashed lines in the Landau region below $\Theta \cong 0.8$ is the same as that of the $RbCaF_3$ data.

data are consistent with such an octahedral rotation, and we assume this model to apply in $RbCaF_3$.

The birefringence Δn will be an even function of ψ, and to lowest order we may take $\Delta n \propto \psi^2$.[19] Similarly, the inversion symmetry at the divalent site requires that the crystal-field expansion determining b_2^0 for the substitutional Fe^{3+} ion contain only even powers of ψ, and for small rotations we expect $b_2^0 \propto \psi^2$.[12] If ψ is described by a critical exponent, $\psi \propto \epsilon^\beta$ where $\epsilon = 1 - (T/T_c)$, then a plot of b_2^0 or Δn vs $\Theta = T/T_c$ will reveal values of β. The result is shown as Fig. 10. Δn is very closely proportional to b_2^0 implying that both have essentially the same dependence on ψ^2 over a rather large temperature range. Recent measurements of the birefringence in $SrTiO_3$ imply that Δn deviates from ψ^2 due to fluctuations.[9] Any such deviation in the case of $RbCaF_3$ appears small.

Figure 10 also shows (as is typical of the other cases)[12,19] a critical region near T_c merging smoothly with a mean-field region in which ψ^2 varies linearly with Θ. Landau theory predicts $\beta = 0.5$,[25] so that both b_2^0 and Δn should vary as $(T_c - T)$ if critical fluctuations are not important. Figure 10 shows this to be the case for $(T/T_c) \lesssim 0.85$ in $RbCaF_3$.

The critical region between $1 > (T/T_c) \gtrsim 0.85$ can be interpreted by procedures identical to those used for $SrTiO_3$,[12] $LaAlO_3$,[12] and $KMnF_3$.[19] It is expected that $\beta \cong 0.33$ for this region, so a plot of $(b_2^0)^{3/2}$ and $(\Delta n)^{3/2}$ vs $(T_c - T)$ should yield a straight line. Figure 11 shows our data plotted in this way. To the accuracy available, $\beta = \frac{1}{3}$ clearly produces an acceptable description in the region from $10 < (T_c - T) < 45$ K, in agreement with the birefringence data shown in Fig. 4. This result compares favorably with the value $\beta = 0.313 \pm 0.004$ computed using the three-dimensional Ising model.[25] However, this straight-line fit does not extend all the way to $\psi^3 = 0$ as in the case of $SrTiO_3$ and $LaAlO_3$, nor does it exhibit a discontinuity as for $KMnF_3$. In fact, the region from $0 \lesssim (T_c - T) \lesssim 10$ K is described quite well by $\beta = 0.25$, as is shown clearly in the inserts of Figs. 3(a) and 6. [A plot of $(\Delta n)^2$ and $(b_2^0)^2$ vs $(T_c - T)$ gives a straight-line fit which extrapolates directly to T_c.] Extrapolation of $(\Delta n)^{3/2}$ and $(b_2^0)^{3/2}$ vs $(T_c - T)$ yields a temperature intercept, $T_a = 201$ K, 3° higher than the observed T_c. In $KMnF_3$ a similar extrapolation[19] gave $T_a - T_c = 1.5$ K, for the discontinuity associated with the small first-order transition which precedes the critical region, while in $SrTiO_3$ and $LaAlO_3$ (both second-order transitions) the extrapolation[12] gives T_c exactly.

We have included in Fig. 10 curves which represent plots of ψ^2 vs T/T_c deduced from the published data for the cases described above, normalized to the same slope in the Landau region. One sees that the linear region for $RbCaF_3$ extrapolates to a value $T/T_c = 1.11$ which is intermediate to the other cases. There is clearly no way to scale these three cases so as to obtain agreement in ψ^2 vs T/T_c as was possible for $SrTiO_3$ and $LaAlO_3$.[12] This suggests the possibility that $RbCaF_3$ may have a weak first-order contribution to the transition at 198 K.

Although neither the relatively large region described by $\beta \simeq 0.25$ (~10 K) nor the apparent lack of hysteresis are compatible with a first-order phase change, this may nevertheless be the case. Similar assignments of $\beta \simeq 0.25$ very near the 186-K transition in $KMnF_3$ were made, based upon both x-ray scattering[26] and birefringence measurements,[6] however, subsequent measurements[19,27] implicated a small first-order contribution to the transition. In any case, it definitely appears that

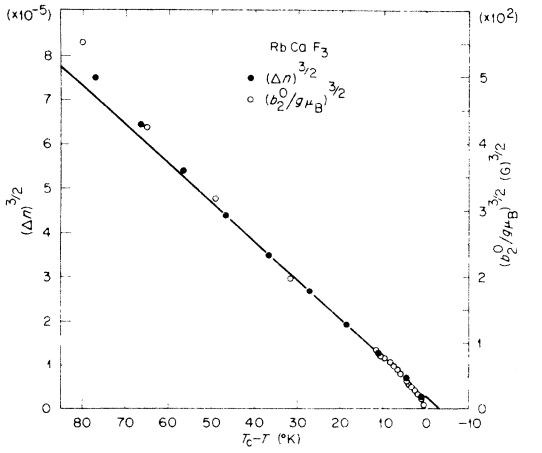

FIG. 11. Temperature dependence of $(b_2^0)^{3/2}$ and $(\Delta n)^{3/2}$ near the transition temperature.

a description of the $RbCaF_3$ 198-K phase change as a simple second-order transition is not possible. It is clearly desirable to follow the temperature dependence of this transition by means of other experiments in order to establish its exact nature. Careful specific-heat experiments might show more clearly whether or not the transition is accompanied by a small latent heat.[28]

B. Low-temperature behavior

The dielectric-constant results show most clearly that additional transitions occur at low temperature. The loss measurements, in particular, suggest transitions at 43 and ~10 K with associated hysteresis. That these effects are related to lattice transition is confirmed by the specific-heat measurements and the anomalous behavior observed in the EPR.

The general forms of the dielectric behavior and hysteresis at 43 K, depicted in Fig. 7, are similar in appearance to the corresponding properties in $PbZrO_3$ near the antiferroelectric transition at 233 K.[29] However, $RbCaF_3$ does not exhibit the large dielectric constant observed for $PbZrO_3$ and typical ($\epsilon \sim 10^3$–10^4) for other oxide perovskites. Nor does $RbCaF_3$ exhibit the typical (for oxide perovskites)[17,27] Curie-Weiss shape above the transition, but decreases only about 10%.

It is possible that the dielectric behavior of $RbCaF_3$ is similar to that observed in rare-earth molybdates, which develop reversible macroscopic electric polarization but no appreciable dielectric enhancement.[30] Such "ferroelectric" behavior is the result of soft-mode condensation of a zone boundary phonon leading to atomic displacements which are reversed in direction in adjacent unit cells.[31]

Finally, it is remarkable that a distinct dielectric loss and change of ϵ is observed at ~10 K, which correlates well with the occurrence of large changes in the EPR spectrum of Fe^{3+}. If these effects are indeed due to a lattice transition, it involves a small free energy and may exhibit quite large hysteresis and other interesting properties.

ACKNOWLEDGMENTS

We would like to thank M. M. Abraham for numerous discussions regarding the EPR measurements and for the use of unpublished calculations. The availability of a capacitance bridge was extremely helpful and we especially appreciate O. E. Schow's assistance in these measurements.

†Research sponsored by the U. S. Atomic Energy Commission under contract with Union Carbide Corporation.

*Permanent address: Department of Physics, University of Kansas, Lawrence, Kan. 66045.

[1]See, for example the Proceedings of the Second European Congress on Ferroelectricity (Dijon) (unpublished) and J. Phys. (Paris) Suppl. 33, (1972) or the Proceedings of the Second International Meeting on Ferroelectricity (Kyoto), (unpublished) and J. Phys. Soc. Jap. Suppl. 28, 1 (1970).

[2]E. F. Steigmeir and H. Anders, Solid State Commun. 12, 565 (1973) and references therein.

[3]Oak Ridge National Laboratory Report No. 2548, 1959, (unpublished).

[4]W. Kanzig, Solid State Phys. 4, 1 (1957) and references therein.

[5]F. W. Lytle, J. Appl. Phys. 35, 2212 (1964).

[6]K. S. Aleksandrov and L. M. Reshchikova, Kristallografiya 14, 716 (1969) [Sov. Phys.—Crystallogr. 14, 614 (1970)].

[7]E. H. Izen and F. A. Modine, Rev. Sci. Instrum. 43, 1563 (1972).

[8]F. A. Modine, R. W. Major, and E. Sonder (unpublished).

[9]E. Courtens, Phys. Rev. Lett. 26, 851 (1971).

[10]L. Rimai and G. A. deMars, Phys. Rev. 127, 702 (1962).

[11]H. Unoki and T. Sakudo, J. Phys. Soc. Jap. 23, 546 (1967).

[12]K. A. Müller and W. Berlinger, Phys. Rev. Lett. 26, 13 (1971).

[13]K. A. Müller, Helv. Phys. Acta 31, 173 (1958).

[14]K. W. H. Stevens, Proc. Phys. Soc. Lond. A65, 209 (1952); also, D. A. Jones, J. M. Baker, and D. F. Pope, Proc. Phys. Soc. Lond. 74, 249 (1959).

[15]T. Sakudo and H. Unoki, Phys. Rev. Lett. 26, 851 (1971).

[16]G. Birnbaum and J. Franeau, J. Appl. Phys. 20, 817 (1949) and references therein.

[17]R. C. Neville, B. Hoeneisen, and C. A. Mead, J. Appl. Phys. 43, 2124 (1972).

[18]K. A. Müller, W. Berlinger and F. Waldner, Phys. Rev. Lett. 21, 814 (1968).

[19]S. Hirotsu and S. Sawada, Solid State Commun. 12, 1003 (1973).

[20]This notation assumes that the origin is at a Ca ion. The notation Γ_{25} refers to the same mode if the origin is taken at a Rb ion.

[21]P. A. Fleury, J. F. Scott, and J. M. Worlock, Phys. Rev. Lett. 21, 16 (1968).

[22]G. Shirane and Y. Yamada, Phys. Rev. 177, 858 (1969).

[23]J. D. Axe, G. Shirane, and K. A. Müller, Phys. Rev. 183, 820 (1969).

[24]J. F. Scott, Phys. Rev. 183, 823 (1969).

[25]L. P. Kadanoff, W. Götze, D. Hamblen, R. Hecht, E. A. S. Lewis, V. V. Palciauskas, M. Rayl, J. Swift, D. Aspnes, and J. Kane, Rev. Mod. Phys. 39, 395 (1967).

[26]V. J. Minkiewicz, Y. Fujii, and Y. Yamada, J. Phys. Soc. Jap. 28, 443, (1970).

[27]L. A. Pozdnyakova, A. I. Kruglik, and K. S. Aleksandov, Kristallografiya 17, 336 (1972) [Soviet Phys.—Crystallogr. 17, 284 (1972)].

[28]M. Furukawa, Y. Fujimori, and K. Hirakawa, J. Phys. Soc. Jap. 29, 1528 (1970).

[29]G. Shirane, E. Swaguchi, and Y. Takagi, Phys. Rev. Lett. 21, 812 (1968).

[30]L. A. Cross, A. Fuskova, and S. E. Cummins, Phys. Rev. Lett. 21, 812 (1968).

[31]J. D. Axe, B. Dorner, and G. Shirane, Phys. Rev. Lett. 26, 519 (1971).

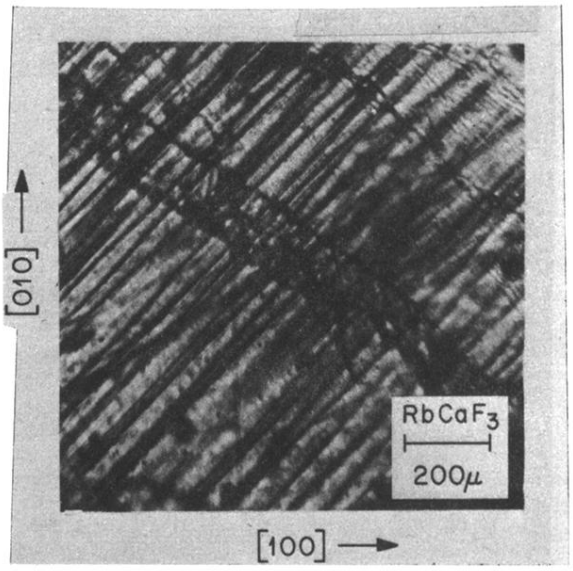

FIG. 1. Typical domain pattern of $RbCaF_3$ below 198 K.